IEEE Photonics Journal
An IEEE Photonics Society Publication

Open Access

Novel CMOS-Compatible Athermal and Polarization-Insensitive Ring Resonator as Photonic Notch Filter

Volume 10, Number 06, December 2018

Francesco Dell'Olio
Donato Conteduca
Giuseppe Brunetti
Mario N. Armenise
Caterina Ciminelli

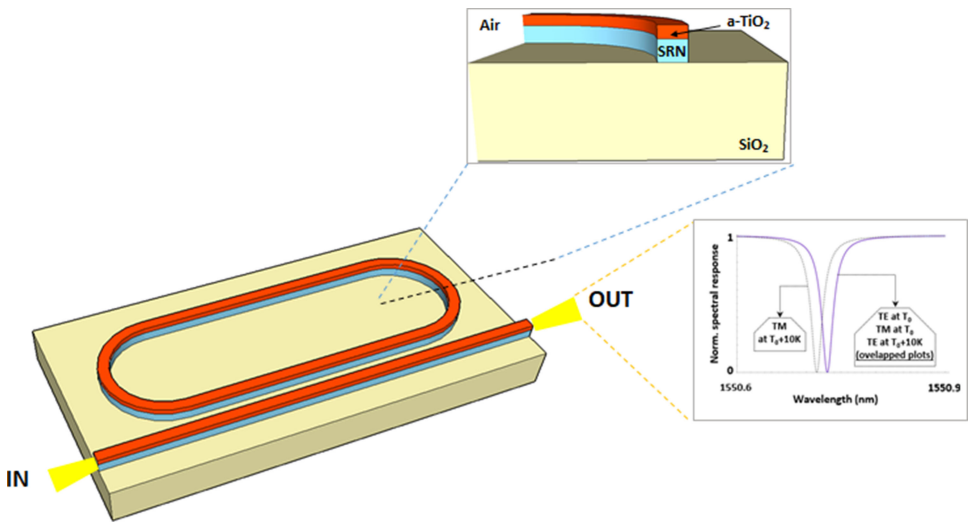

DOI: 10.1109/JPHOT.2018.2877081
1943-0655

Novel CMOS-Compatible Athermal and Polarization-Insensitive Ring Resonator as Photonic Notch Filter

Francesco Dell'Olio, Donato Conteduca, Giuseppe Brunetti, Mario N. Armenise, and Caterina Ciminelli

Optoelectronics Laboratory, Politecnico di Bari, Bari 70125, Italy

DOI:10.1109/JPHOT.2018.2877081

Manuscript received August 22, 2018; revised October 11, 2018; accepted October 14, 2018. Date of publication October 19, 2018; date of current version November 12, 2018. Corresponding author: Caterina Ciminelli (e-mail: caterina.ciminelli@poliba.it).

Abstract: A hybrid titanium dioxide/silicon rich nitride ring resonator with the unique feature of being simultaneously athermal and polarization-insensitive is reported for the first time to our knowledge. Although its potential application domain is extremely wide, the designed integrated microphotonic cavity, having a racetrack shape, is intended for notch filtering in a microwave photonic passband filter. A careful selection of the CMOS-compatible material system and an innovative design approach have allowed a very low dependence of the filtering shape on the input beam polarization and, simultaneously, a thermal drift of the resonance wavelength $<$1.5 pm/K. The numerically estimated Q-factor, free spectral range, and extinction ratio are compliant with the requirements of the selected application, being equal to 7.8×10^4, 4 nm, and 30.7 dB, respectively.

Index Terms: Integrated photonic systems, waveguide devices.

1. Introduction

Planar ring resonators (RRs) [1] are key integrated microphotonic components that are widely used in many application domains, such as fiber telecommunications (e.g., add/drop multiplexers, switches, laser wavelength lockers) [2], [3], sensing (e.g., biosensors, optoelectronic gyros) [4], [5], and microwave photonics (e.g., true time delay lines, microwave filters, optoelectronic oscillators, frequency combs generators) [6]–[8]). CMOS-compatible RRs [9]–[12], mainly silicon and silicon nitride RRs, have very interesting features such as low cost, small size, high Q-factor, and easy manufacturing. However, they are typically quite sensitive to temperature, with a typical resonance wavelength drift in the range 10–100 pm/K [13], [14]. In addition, CMOS-compatible RRs are very sensitive to the polarization of the input beam, and therefore they are usually designed for a specific polarization of the input beam (TE or TM).

Several CMOS-compatible athermal RRs, which are not polarization-insensitive, have been reported in literature [15]–[20]. In particular, a hybrid TiO_2/Si_3N_4 RR with a temperature-dependent resonance wavelength drift of the order of only 0.1 pm/K, a radius of 200 μm, a free spectral range of 0.9 nm, and a high Q-factor of 155,000 has been demonstrated in [21].

Some polarization-insensitive RRs in CMOS-compatible material systems have been demonstrated [22]–[24]. These components, which are all not athermal, are based on properly engineered rib or slot waveguides and evanescent or multimode-interference couplers. The best experimental

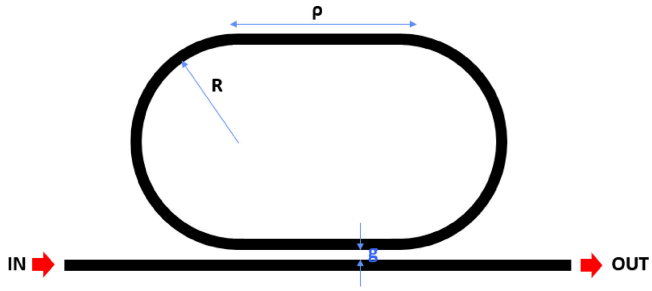

Fig. 1. Configuration of the racetrack resonator. *R* is the bending radius, ρ is the length of the straight sections, and *g* is the bus waveguide/resonator gap.

value of Q = 90,000 has been achieved in a silicon polarization-insensitive racetrack resonator with length of about 3,500 μm [25].

For eliminating the polarization dependence in RRs, the so-called polarization diversity scheme can be used [26]. According to this approach, a polarization-insensitive RR can be implemented by two identical polarization-sensitive rings, a polarization splitter, a polarization combiner, and a polarization rotator. In this way, the polarization transparency is achieved at the expense of an increase of the device complexity.

To our knowledge, no RR that is simultaneously athermal and polarization-insensitive has been reported so far in literature.

Here we report on the design of a novel CMOS-compatible planar resonant cavity with a racetrack shape (see Fig. 1), which is simultaneously athermal and polarization-insensitive. Although we have used modelling and design techniques already reported in literature, we would like to stress that the achievement of both these key feature is surely not trivial. In fact, it implies the selection of a realistic material system including materials with opposite thermo-optic coefficients, the proper design of an athermal waveguide having also an extremely low birefringence, and the optimization of a bus waveguide/resonator evanescent coupler having the same efficiency for both the polarizations.

A RR that is athermal and polarization-insensitive can be very useful in the field of biosensing, microwave photonics, and fiber telecommunication, because its spectral response does not change with the polarization of the input beam and it is not affected by the temperature drift. We assume the operating wavelength of the resonator equal to 1.55 μm.

The designed component is a notch photonic filter, to be utilized in a microwave signal filtering subsystem. In fact, by using the approach in [27], a passband microwave filter with high performance can be implemented by using a laser source, a phase modulator, a photonic notch filer, and a photodiode. The design strategy presented here is very general and can be used to design athermal and polarization-insensitive RR for any other application.

The racetrack shape instead of the circular one has been selected for the resonator because, as it will be shown in the section 3, the circular shape does not allow realizing the polarization-insensitivity condition.

The two building blocks of the athermal and polarization-insensitive RR are the waveguide and the bus waveguide/resonator evanescent coupler.

In a RR, the temperature dependence of the resonant wavelength λ_0 is given by [15], [21]:

$$\frac{\partial \lambda_0}{\partial T} = \left(n_{eff} a_{sub} + \frac{\partial n_{eff}}{\partial T} \right) \frac{\lambda_0}{n_g} \tag{1}$$

where T is the temperature, n_{eff} is the waveguide effective index, a_{sub} is the substrate expansion coefficient, and n_g is the group index of the waveguide. The athermality condition is achieved when $\partial \lambda_0 / \partial T$ is zero. The only way to obtain this condition is that the following equation is verified for both polarizations:

$$\frac{\partial n_{eff}}{\partial T} = -n_{eff} a_{sub}. \tag{2}$$

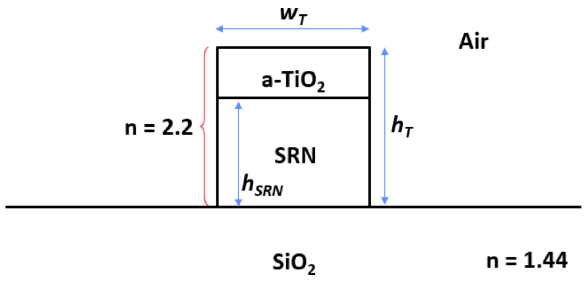

Fig. 2. Cross-section of the designed waveguide. The Si substrate on which the SiO_2 layer is grown is not shown. a-TiO_2: amorphous TiO_2. n: refractive index.

To make the resonator simultaneously athermal and polarization-insensitive the following conditions should be also verified: i) the waveguide must support only the fundamental quasi-TE and quasi-TM modes; ii) the effective index of the two modes ($n_{eff,TE}$ and $n_{eff,TM}$) must be the same, i.e., zero birefringence. The evanescent coupler must have the same efficiency for both polarizations ($\eta_{TE} = \eta_{TM}$) and the drift of the coupling efficiency due to temperature must be zero for both polarizations. The designed resonator has features very close to the above-mentioned requirements.

2. Waveguide Configuration and Design

The design of an athermal CMOS-compatible RR, which requires Eq. (2) satisfaction, implies the use of a material with negative thermo-optic coefficient (TOC) together with materials with positive TOC. In fact, when T increases (decreases) the materials with positive TOC exhibit an increase (decrease) of the refractive index, while the material with negative TOC shows a decrease (increase) of the refractive index. By an appropriate design of the RR waveguide, the compensation of the two physical effects can be achieved.

We have selected the amorphous titanium dioxide (TiO_2) as material with negative TOC. TiO_2 is a CMOS-compatible material having a good chemical stability and biocompatibility. It has been widely used in micro- and nano-electronics [28], [29] and integrated microphotonics [30].

At 1.55 μm, the refractive index of the amorphous TiO_2 is 2.2 [15]. To make the resonator polarization insensitive we have considered as core material the positive TOC silicon-rich silicon nitride (SRN), whose most interesting feature in the context of our design is that its refractive index can be tailored to be matched to that one of the titanium dioxide. In fact, the refractive index of SRN, which is an emerging photonic material that is transparent at 1.55 μm [31], can be finely adjusted by varying the N/Si ratio during the film deposition process [31]. In particular, the SRN has a refractive index of 2.2 if the N/Si ratio is 1.1 [31].

We assume that the amorphous film of SRN, with a N/Si ratio of 1.1 and a refractive index of 2.2, is deposited by low-pressure chemical vapor deposition on a 2 μm thick thermally-grown SiO_2 layer (refractive index $=$ 1.44 at 1.55 μm) [32]. In addition, we assume that the SiO_2 layer is grown on a Si substrate and that the amorphous titanium dioxide layer is deposited by low temperature RF magnetron sputtering, which allows the deposition of a very smooth TiO_2 layer having a standard deviation of the roughness $<$1 nm [33].

The cross-section of the designed waveguide is a plasma etched TiO_2/SRN multi-layer, as shown in Fig. 2 [32], [34]. The use of the selected material system for manufacturing integrated optical devices was already experimentally proved [21], the fabrication process including standard steps have been clearly envisaged. We have verified that the device geometrical dimensions that we have considered in the design are compatible to this process.

The thickness of the SRN layer is denoted as h_{SRN}, the total thickness of the TiO_2/SRN multi-layer is h_T, and the waveguide width is w_T.

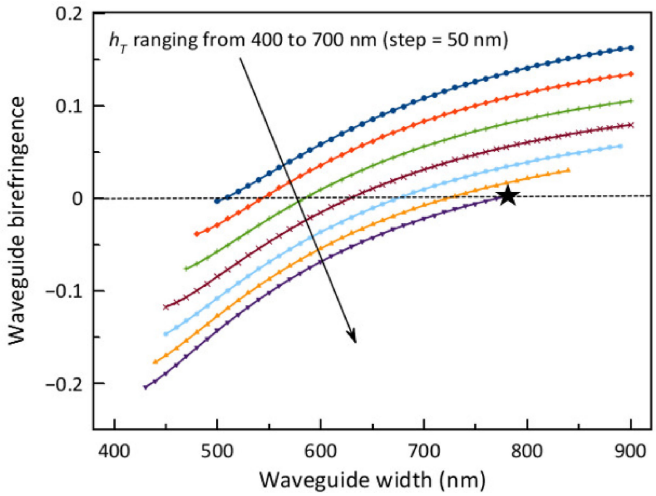

Fig. 3. Waveguide birefringence ($= n_{eff,TE} - n_{eff,TM}$) dependence on the waveguide width for h_T ranging from 400 to 700 nm (step = 50 nm). The star indicates the optimum condition. The upper curve (blue) is for $h_T = 400$ nm and h_T gradually increases with a step of 50 nm in the other curves, according to the versus of the arrow.

The geometrical features w_T and h_T have been optimized aiming at achieving the condition $n_{eff,TE} = n_{eff,TM}$, i.e., birefringence = 0, while the thickness of the SRN layer h_{SRN} has been chosen to have an effective TOC of the waveguide equal to $-n_{eff}\ a_{sub}$ (being a_{sub} equal to $2.6 \times 10^{-6}\ K^{-1}$ [21]).

The effective index of the waveguide has been calculated by the finite element method (FEM). A very fine mesh has been used (the elements size in the waveguide core is 1 nm). The number of degrees of freedom is the effective index computation is of the order of 10^6.

The dependence of the waveguide birefringence on w_T for several values of h_T is shown in Fig. 3. The considered values of h_T and w_T are those for which the waveguide supports only the fundamental quasi-TE and quasi-TM modes. The birefringence depends only on w_T and h_T, sum of the thickness of the TiO_2 layer ($h_T - h_{SRN}$) and the thickness of the SRN layer (h_{SRN}). This means that for a given couple of values of w_T and h_T, the birefringence is independent of the thickness of the TiO_2 and SRN layers.

As expected, the birefringence $B = n_{eff,TE} - n_{eff,TM}$ increases as w_T increases. B decreases as h_T increases. For all values of h_T that we have considered there is a value of w_T assuring the achievement of the zero-birefringence condition. To minimize the waveguide birefringence due to potential fabrication tolerances on w_T we have calculated $\partial B/\partial w_T$ for all values of w_T fulfilling the zero-birefringence condition. The minimum value of the derivative ($<10^{-4}\ nm^{-1}$) has been obtained for $w_T = 770$ nm. Thus, the selected values of h_T and w_T have been 700 nm and 770 nm, respectively.

As already mentioned, the thickness of the SRN layer (h_{SRN}) has been engineered aiming at achieving the condition shown in Eq. (2), i.e., effective TOC $= -n_{eff}\ a_{sub}$ (or, equivalently, effective TOC $+ n_{eff}\ a_{sub} = 0$) for both the polarizations.

The assumed TOC values for SRN with refractive index = 2.2 (N/Si ratio = 1.1), SiO_2, and TiO_2 are $4 \times 10^{-5}\ K^{-1}$, $1.5 \times 10^{-5}\ K^{-1}$, and $-1 \times 10^{-4}\ K^{-1}$, respectively [37], [15]. The plot of the sum (effective TOC $+ n_{eff}\ a_{sub}$), which must be equal to zero according to Eqs. (1) and (2), vs. h_{SRN} is shown in Fig. 4.

The sum (effective TOC $+ n_{eff}\ a_{sub}$), which is directly proportional to the wavelength shift due to the temperature drift (see Eq. (1), increases as h_{SRN} increases. In fact, for low values of h_{SRN} the thickness of the TiO_2 film $= (h_T - h_{SRN})$ is larger than the thickness of the SRN film and consequently the optical mode is more confined in the material having a negative TOC than in the material having a positive TOC. Thus, for low values of h_{SRN}, the effective TOC is negative and one order of magnitude larger than $n_{eff}\ a_{sub}$ (this quantity is of the order of 10^{-6}). As h_{SRN}

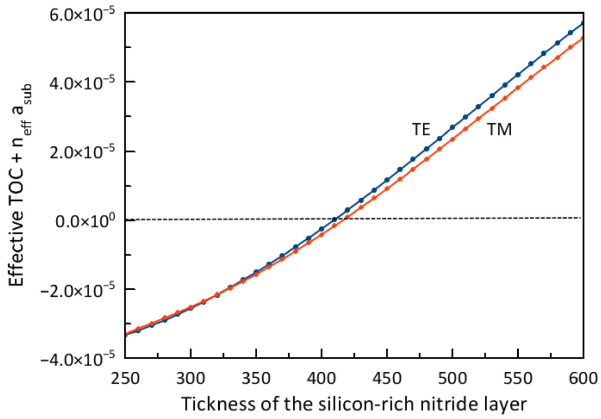

Fig. 4. Effective TOC dependence on h_{SRN}. The total thickness of the waveguide h_T is 700 nm. The thickness of the TiO_2 layer is $h_T - h_{SRN}$. The waveguide with is 770 nm.

increases, the confinement in the material having a positive TOC increases and the effective TOC increases, too. For the TE mode, the sum (effective TOC + n_{eff} a_{sub}) is very close to zero ($= 2 \times 10^{-9}$ K^{-1}) for $h_{SRN} = 440$ nm. For that value of h_{SRN}, the sum (effective TOC + n_{eff} a_{sub}) for the TM mode is not exactly zero but is very low ($= -1.8 \times 10^{-6}$ K^{-1}). Consequently, the waveguide having $h_{SRN} = 440$ nm is very close to the exact athermality condition. The TM mode is more sensitive than TE mode on temperature because the selected value of h_{SRN} allows the exact fulfilment of the athermality condition only for the TE polarization, while, for the TM mode, the h_{SRN} value implies a value of the sum (effective TOC + n_{eff} a_{sub}) that is slightly far from zero (of the order of 10^{-6} K^{-1}). As it is evident from Fig. 4, no value of h_{SRN} allows the exact fulfilment of the athermality condition for both the polarizations.

We have carefully investigated the distribution of the optical field in the optimized waveguide having $h_T = 700$ nm, $w_T = 770$ nm, $h_{SRN} = 440$ nm, thickness of the TiO_2 layer $= h_T - h_{SRN} =$ 260 nm. The field is mainly confined in SRN layer (54.84% for the TM mode and 56.21% for the TE mode) than in the TiO_2 layer (21.97% for the TM mode and 23.21% for the TE mode). We verified that these values of confinement factor in the SRN layer and the TiO_2 layer are the best ones for the achievement of the athermality condition.

The scattering loss of the optimized waveguide been calculated by the 3D current volume method [34], [35], using a standard exponential model for the autocorrelation function describing the roughness. According to [31], we have assumed that the roughness of the SRN film has a standard deviation of 0.5 nm. The film of amorphous TiO_2 is deposited on this very smooth surface. At the TiO_2/SRN rough interface no chemical reaction occurs. It is an amorphous-amorphous interface introducing only scattering loss due to the roughness of the two surfaces forming the interface. Assuming the above-mentioned value of the roughness standard deviation, we have calculated the scattering loss due to the TiO_2/SRN rough interface by the 3D current volume method (a standard exponential model has been used for the autocorrelation function describing the roughness) [25], [36]. We have found that this loss is $<$0.1 dB/cm.

We have verified that the waveguide loss is mainly due to the roughness of the waveguide vertical sidewalls. The parameters of this roughness are standard deviation $= 5$ nm and correlation length $= 45$ nm [32]. The numerically estimated scattering loss is 1.51 dB/cm for the TM mode and 1.54 dB/cm for the TM mode.

To select the radius of the bent sections of the racetrack resonator, the bending loss of the optimized waveguide has been calculated by the finite element method solving the Maxwell equations in a cylindrical coordinate system [38]. The bending loss (log. scale) dependence on the curvature radius R is shown in Fig. 5.

As expected, the bending loss exponentially decreases as R increases. To have a bending loss $<$0.01 dB/cm the radius must be >7 μm. We have chosen $R = 8$ μm.

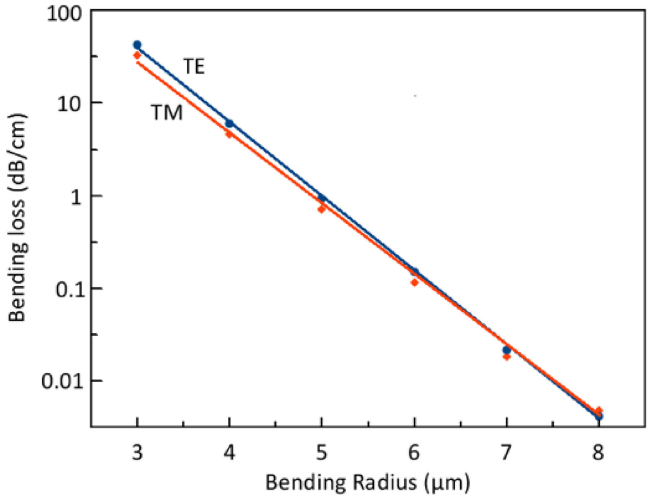

Fig. 5. Bending loss (log. scale) dependence on the curvature radius for the optimized waveguide having $h_T = 700$ nm, $w_T = 770$ nm, and $h_{SRN} = 440$ nm.

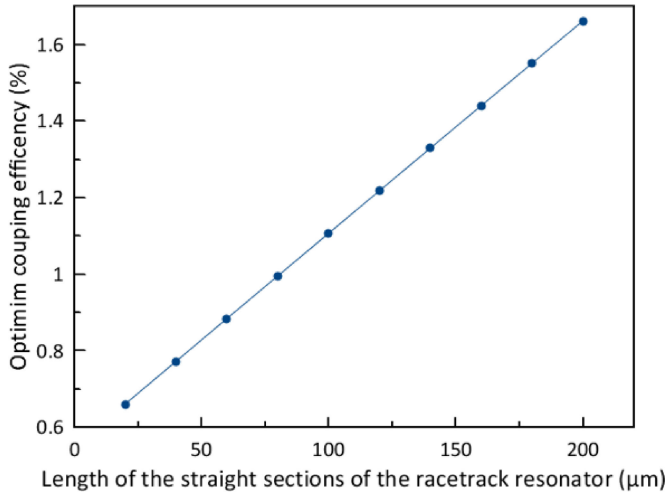

Fig. 6. Optimum value of η vs. ρ.

3. Ring Resonator Design

The spectral response of the resonator, its Q-factor, and its extinction ratio (ER) have been calculated by the well-established model in [39]. For the design of the evanescent coupler we have used the modelling approach in [40], which is based on the coupled-mode theory (CMT) applied to the case in which the coupling coefficient varies in the propagation direction [41].

The selected application, i.e., optical notch filtering in a microwave photonic passband filtering subsystem, requires a high value of ER ($\geq$20 dB) and a Q-factor $>$10,000 because, as discussed in [27], this performance parameter of the optical notch filter has a strong impact on the overall performance of the microwave pass band filter. In addition, the target application demands a very good thermal stability of the optical notch filter, as clearly pointed out in [27]. The target value of ER for the designed racetrack resonator is 20 dB. Assuming $R = 8$ μm, an evanescent coupler loss $=$ 0.5%, and requiring ER $=$ 20 dB, the optimum value of the bus/ring coupling efficiency (η) has been calculated for a length of straight sections of the racetrack resonator (ρ) ranging from 20 to 200 μm (see Fig. 6). The optimum value of η does not depend on the polarization of the input beam (TE or TM) because the TE and the TM mode have practically the same loss.

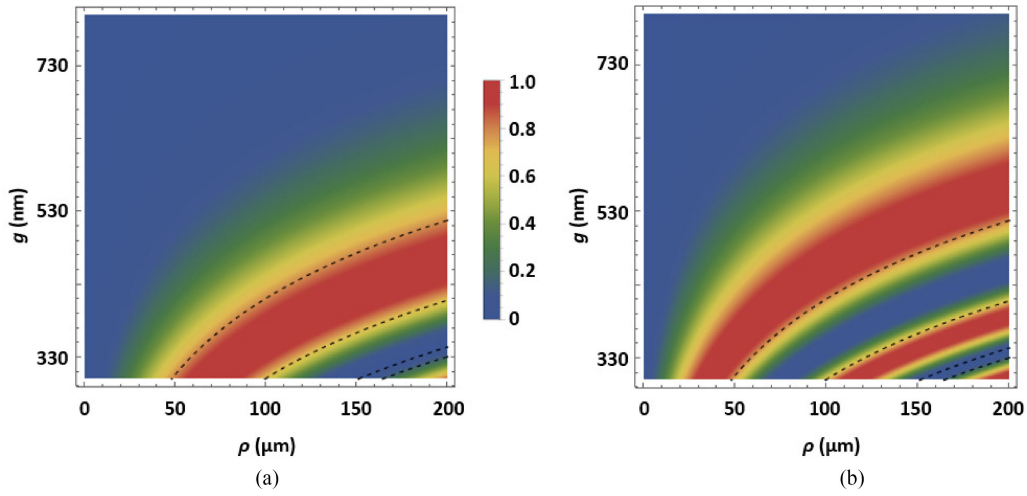

Fig. 7. Contour plots of the coupling efficiency dependence on the length of the straight sections of the racetrack ρ and the bus/resonator gap g. (a) TE mode. (b) TM mode. The gap g varies in the range 300 nm–800 nm while ρ varies in the range 0 μm–200 μm.

The optimum value of the coupling efficiency η increases as ρ increases because when ρ increases the round-trip loss in the resonant path increases, too. To compensate this increase of the round-trip loss keeping ER = 20 dB the coupling efficiency η must be increased. From Fig. 6 we can observe that the optimum value of the bus/ring coupling efficiency is in the range 0.66%–1.66% for ρ in the range 20–200 μm.

By using the CMT-based modelling approach as in [40] we have numerically investigated the dependence of η_{TE} and η_{TM} on the two geometrical parameters of the evanescent coupler, i.e., ρ and the bus/ring gap (g). The contour plot showing the η dependence on ρ and g for the TE and the TM modes is in Fig. 7. The dashed lines in the contour plot highlight the condition $\eta_{TE} = \eta_{TM}$. From the contour plot it is evident that, for $\rho = 0$, is not possible to achieve the condition $\eta_{TE} = \eta_{TM}$ that makes the evanescent coupler polarization insensitive. This is the reason why we have selected a racetrack shape instead of a circular one for the resonator.

As expected, for both polarizations, the coupling efficiency decreases as g increases and η shows a periodic dependence on ρ, as in case of an evanescent coupler formed by two parallel straight waveguides.

In the design of the coupler, we must choose a couple of values of ρ and g for which $\eta_{TE} = \eta_{TM}$ (dashed lines in the contour plots shown in Fig. 7). In addition, the coupling efficiency ($\eta_{TE} = \eta_{TM}$) must be as close as possible to the optimum one (for each value of ρ there is an optimum value of coupling efficiency η, as shown in Fig. 6).

The closest condition to the optimum one is achieved for $\rho = 151$ μm and $g = 300$ nm. For this couple of values, we have $\eta_{TE} = \eta_{TM} = 1.6\%$.

Assuming $\rho = 151$ μm and $g = 300$ nm, the spectral response of the resonator for both the polarizations and for $T_0 = 300$ K and $T_0 + 10$ K is shown in Fig. 8.

The plot in Fig. 8 shows a very good insensitivity of the racetrack resonators to temperature drift and polarization state of the input beam (all the spectra are overlapped). The resonator has a free spectral range (FSR) of 4 nm, a Q-factor of 78,300 and ER = 30.7 dB (10.7 dB higher than the target one). FSR, Q-factor, and ER are practically the same for the two polarizations (difference $<1\%$). For the TE mode, the resonance wavelength shift due to the temperature drift is $<<0.1$ pm/K. The same parameter is 1.5 pm/K for the TM mode. At T_0, the resonance wavelength is practically the same for the TE and the TM mode. At $T_0 + 10$K, the difference between the TE and the TM resonance is approximately 15 pm. This is due to the nonzero value of the sum (effective TOC + n_{eff} a_{sub}) of the waveguide for the TM polarization (as mentioned in section 2, the sum effective TOC + n_{eff} a_{sub} is -1.8×10^{-6} K^{-1} for the TM mode). The effect of the nonzero value of the sum (effective

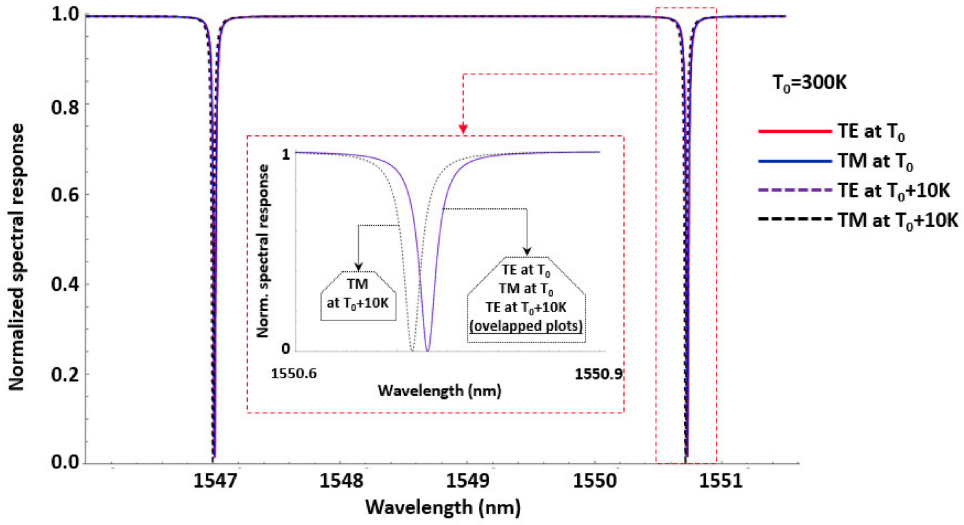

Fig. 8. Spectral response of the designed resonator for both the polarizations and for T0 = 300 K and T0 + 10 K. The inset shows a zoom of the spectra in the wavelength range 1550.6 nm–1550.9 nm.

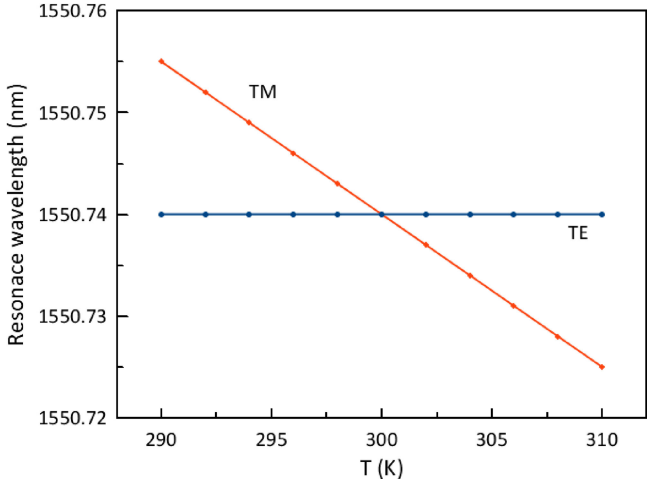

Fig. 9. Resonance wavelength dependence on T for both polarizations.

TOC + n_{eff} a_{sub}) is also shown in Fig. 9, where the resonator resonance wavelength vs. T is plotted for both polarizations. At $T_0 = 300$ K the resonance wavelength is the same for TE and TM modes, confirming that the cavity is polarization insensitive. As T varies, the resonance wavelength for TE mode remains practically constant while the resonance wavelength for TM mode decreases as T increases. Therefore, as T drifts from T_0, we can observe a slight perturbation of the polarization insensitivity condition.

The optimized geometrical parameters and the performance of the designed resonator are summarized in Table 1. The achieved ER is larger than the target one and the calculated Q-factor is compliant with the requirement imposed by the specific application.

By FEM, we have calculated the waveguide birefringence B for 1,000 times when w_T is equal to (770 nm + u) and h_T is equal to (700 nm + v), being u and v random numbers that are drawn from a normal distribution having a mean of 0 and standard deviation of 2.5 nm. This means that approximately 95% of the 1,000 values of w_T and h_T are in the range (nominal value ± 5 nm). The mean value of B is very close to zero (3.2×10^{-8}), the standard deviation of B is 3.3×10^{-5}, and the worst-case value of |B| is 1.0×10^{-4}. In all iterations, we calculated both the TE and

TABLE 1
Geometrical and Performance Parameters of the Designed Resonator

Parameter	Symbol	Value
Thickness of the SiO_2 layer	-	3.00 μm
Thickness of the SRN layer	h_{SRN}	0.44 μm
Thickness of the TiO_2 layer	-	0.26 μm
Total thickness of the TiO_2/SRN multi-layer	h_T	0.70 μm
Waveguide width	w_T	0.77 μm
Length of the straight sections of the resonator	ρ	151 μm
Bending radius of the bent sections of the resonator	R	8.00 μm
Bus/ring gap	g	0.30 μm
Q-factor	-	78,300
Extinction ratio	ER	30.7 dB
Free spectral range	-	4 nm
Thermal drift of the resonance wavelength (TE mode)	-	<< 0.1 pm/K
Thermal drift of the resonance wavelength (TM mode)	-	1.5 pm/K

the TM resonance wavelength. The maximum difference between the TE and the TM resonance wavelength is $<$0.1 nm.

We have calculated the resonance wavelength shift due to the temperature drift for 1,000 times when w_T is (770 nm + u), h_T is (700 nm + v) and h_{SRN} is (440 nm + w), being u, v, and w random numbers that are drawn from a normal distribution having a mean of 0 and standard deviation of 2.5 nm. The worst-case value of the resonance wavelength shift due to the temperature drift is 4.3 pm/K.

This statistical analysis has allowed us to conclude that, if the waveguide geometrical parameters (w_T, h_T, and h_{SRN}) are in the range (nominal value $\pm$ 5 nm), the maximum difference between the TE and the TM resonance wavelength is $<$0.1 nm. When the waveguide geometrical parameters are in the above-mentioned range, the resonance wavelength shift due to the temperature drift is always $<$5 pm/K.

All the above-reported results have been obtained in the in the wavelength range from 1545 to 1555 nm. In this wavelength range, the resonator is simultaneously polarization insensitive and athermal. In the whole C-band (wavelength range: 1530–1565 nm), the magnitude of the waveguide birefringence is less than 3×10^{-4}. This means that, in this band having a width of 35 nm, the maximum difference between the TE and the TM resonance wavelength is $<$0.3 nm. We have verified that in whole C-band, the resonance wavelength shift due to the temperature drift is always $<$5 pm/K.

4. Conclusions

The design of a novel CMOS-compatible athermal and polarization-insensitive RR has been reported. The most interesting feature of the component, which is highly suitable in many applications,

is the negligible dependence of the spectral response on the input beam polarization and simultaneously the very low dependence of the resonance wavelength and the filtering shape on any thermal drift (max. thermal drift of the resonance = 1.5 pm/K). In literature CMOS-compatible RRs only with an extremely low thermal drift of the resonance ($<$0.1 pm/K) or polarization insensitive are reported. To our knowledge, the device reported here is the first one having both the features. For example, this can be very useful when the resonator is used in the field of add/drop filtering in wavelength division multiplexing systems. In fact, in this context, the thermal stability of the resonance wavelength is required, and the polarization of the filter input beam is unknown and consequently polarization insensitive filters are strongly demanded.

The designed cavity exhibits a performance in terms of Q-factor (= 78,300), free spectral range (= 4 nm), and extinction ratio (= 30.7 dB) that is compliant with the requirements of the selected specific application, i.e., notch filtering in a microwave photonic filter including, in addition to the resonator, a tunable laser diode, a phase modulator, and a photodiode. The design strategy we carried out is very general and can be used for designing other athermal and polarization insensitive integrated microphtotonic components, including optical filters having a multi-ring configuration.

The free spectral range of the notch optical filter can be extended up to several tens of nanometers by using the Vernier effect in a configuration including series-coupled racetrack resonators [42]. In this way, all the performance parameters of the optical filter could match the requirements of the add/drop multiplexing, i.e., Q of the order of 10^4-10^5, extinction ratio $>$30 dB, FSR $>$30 nm.

References

[1] E. A. J. Marcatilli, "Bends in optical dielectric waveguides," *Bell Labs Tech. J.*, vol. 28, pp. 2103–2132, 1969.
[2] B.E. Little, S.T. Chu, H.A. Haus, J.S. Foresi, and J.-P. Laine, "Microring resonator channel dropping filters," *J. Lightw. Technol.*, vol. 15, no. 6, pp. 998–1005, Jun. 1997.
[3] A. Melikyan, G. de Valicourt, K. Kim, N. Fontaine, Y. Chen, and P. Dong, "Hybrid III-V/Silicon laser with integrated athermal wavelength locker," in *Proc. Euro. Conf. Opt. Commun.*, 2017, pp. 1–3.
[4] A. Ksendzov and Y. Lin, "Integrated optics ring-resonator sensors for protein detection," *Opt. Lett.*, vol. 30, pp. 3344–3346, 2005.
[5] C. Ciminelli *et al.*, "A high-Q InP resonant angular velocity sensor for a monolithically integrated optical gyroscope," *IEEE Photon. J.*, vol. 8, no. 1, 2016, Art. no. 6800418.
[6] L. Maleki, "The optoelectronic oscillator," *Nature Photon.*, vol. 5, pp. 728–730, 2011.
[7] D. Conteduca, F. Dell'Olio, C. Ciminelli, and M. N. Armenise, "Resonant graphene-based tunable optical delay line," *IEEE Phton. J.*, vol. 7, no. 6, 2015, Art. no. 7802409.
[8] M.-G. Suh and K. J. Vahala, "Soliton microcomb range measurement," *Science*, vol. 359, pp. 884–887, 2018.
[9] W. Bogaerts *et al.*, "Silicon microring resonators," *Laser Photon. Rev.*, vol. 6, pp. 47–73, 2012.
[10] D. T. Spencer, J. F. Bauters, M. J. R. Heck, and J. E. Bowers, "Integrated waveguide coupled Si_3N_4 resonators in the ultrahigh-Q regime," *Optica*, vol. 1, pp. 153–157, 2014.
[11] X. Ji *et al.*, "Ultra-low-loss on-chip resonators with sub-milliwatt parametric oscillation threshold," *Optica*, vol. 4, pp. 619–624, 2017.
[12] K. Vahala, K. Y. Yang, D. Y. Oh, S. H. Lee, X. Yi, and Q. F. Yang, "An integrated ultra-high-Q resonator for optical clocks, synthesizers, gyroscopes and spectroscopy," in *Proc. IEEE Photon. Conf.*, 2017, pp. 389–390.
[13] T. Baehr-Jones, M. Hochberg, C. Walker, E. Chan, D. Koshinz, W. Krug, and A. Scherer, "Analysis of the tuning sensitivity of silicon-on-insulator optical ring resonators," *J. Lightw. Technol.*, vol. 23, no. 12, pp. 4215–4221, Dec. 2005.
[14] J.-M. Lee, D.-J. Kim, H. Ahn, S.-H. Park, and G. Kim, "Temperature dependence of silicon nanophotonic ring resonator with a polymeric overlayer," *J. Lightw. Technol.*, vol. 25, no. 8, pp. 2236–2243, Aug. 2007.
[15] B. Guha, B. B. C. Kyotoku, and M. Lipson, "CMOS-compatible athermal silicon microring resonators," *Opt. Exp.*, vol. 18, pp. 3487–3493, 2010.
[16] F. Qiu, A. M. Spring, F. Yu, and S. Yokoyama, "Complementary metal–oxide–semiconductor compatible athermal silicon nitride/titanium dioxide hybrid micro-ring resonators," *Appl. Phys. Lett.*, vol. 102, 2013, Art. no. 051106.
[17] B. Guha, J. Cardenas, and M.l Lipson, "Athermal silicon microring resonators with titanium oxide cladding," *Opt. Exp.*, vol. 21, pp. 26557–26563, 2013.
[18] S. S. Djordjevic *et al.*, "CMOS-compatible, athermal silicon ring modulators clad with titanium dioxide," *Opt. Exp.*, vol. 21, pp. 13958–13968, 2013.
[19] J. Bovington, R. Wu, K.-T. Cheng, and J. E. Bowers, "Thermal stress implications in athermal TiO_2 waveguides on a silicon substrate," *Opt. Exp.*, vol. 22, pp. 661–666, 2014.
[20] S. Feng *et al.*, "Athermal silicon ring resonators clad with titanium dioxide for 1.3 μm wavelength operation," *Opt. Exp.*, vol. 23, pp. 25653–25660, 2015.
[21] F. Qiu, A. M. Spring, and S. Yokoyama, "Athermal and High-Q Hybrid $TiO_2-Si_3N_4$ ring resonator via an etching-free fabrication technique," *ACS Photon.*, vol. 2, pp. 405–409, 2015.
[22] D.-X. Xu, S. Janz, and P. Cheben, "Design of polarization-insensitive ring resonators in silicon-on-insulator using MMI couplers and cladding stress engineering," *IEEE Photon. Tech. Lett.*, vol. 18, no. 2, pp. 343–345, Jan. 2006.

[23] Z. Wang, D. Dai, and S. He, "Polarization-insensitive ultrasmall microring resonator design based on optimized Si sandwich nanowires," *IEEE Photon. Technol. Lett.*, vol. 19, no. 20, pp. 1580–1582, Oct. 2007.
[24] M. Erdmanis *et al.*, "Towards broad-bandwidth polarization-independent nanostrip waveguide ring resonators," *Opt. Exp.*, vol. 21, pp. 9974–9981, 2013.
[25] W. R. Headley, G. T. Reed, S. Howe, A. Liu, and M. Paniccia, "Polarization-independent optical racetrack resonators using rib waveguides on silicon-on-insulator," *Appl. Phys. Lett.*, vol. 85, 2004, Art. no. 5523.
[26] T. Barwicz *et al.*, "Polarization-transparent microphotonic devices in the strong confinement limit," *Nature Photon.*, vol. 1, pp. 57–60, 2007.
[27] J. Palaci, G. E. Villanueva, J. V. Galan, J. Marti, and B. Vidal, "Single bandpass photonic microwave filter based on a notch ring resonator," *IEEE Photon. Technol. Lett.*, vol. 22, no. 17, pp. 1276–1278, Sep. 2010.
[28] D. Rathee, S. K. Arya, and M. Kumar, "Analysis of TiO_2 for microelectronic applications: Effect of deposition methods on their electrical properties," *Front. Optoelectron. China*, vol. 4, pp. 349–358, 2011.
[29] S. K. Kim, K. M. Kim, D. S. Jeong, W. Jeon, K. J.Yoon, and C. S. Hwang, "Titanium dioxide thin films for next-generation memory devices," *J. Mater. Res.*, vol. 28, pp. 313–325, 2013.
[30] M. Furuhashi *et al.*, "Development of microfabricated TiO_2 channel waveguides," *AIP Adv.*, vol. 1, 2011, Art. no.032102.
[31] C. Lacava *et al.*, "Si-rich silicon nitride for nonlinear signal processing applications," *Sci. Rep.*, vol. 7, 2017, Art. no. 22.
[32] C. J. Krückel, A. Fülöp, T. Klintberg, J. Bengtsson, P. A. Andrekson, and V. Torres-Company, "Linear and nonlinear characterization of low-stress high-confinement silicon-rich nitride waveguides," *Opt. Exp.*, vol. 23, pp. 25827–25837, 2015.
[33] J. D. B. Bradley *et al.*, "Submicrometer-wide amorphous and polycrystalline anatase TiO_2 waveguides for microphotonic devices," *Opt. Exp.*, vol. 20, pp. 23821–23831, 2012.
[34] M. Häyrinen, M. Roussey, V. Gandhi, P. Stenberg, A. Säynätjoki, and L. Karvonen, "Low-loss titanium dioxide strip waveguides fabricated by atomic layer deposition," *J. Lightw. Technol.*, vol. 32, no. 2, pp. 208–212, Jan. 2014.
[35] C. Ciminelli, V. M. N. Passaro, F. Dell'Olio, and M. N. Armenise, "Three-dimensional modelling of scattering loss in InGaAsP/InP and Silica-on-Silicon bent waveguides," *J. Euro. Opt. Soc.–Rapid Pub.*, vol. 4, 2009, Art. no. 09015.
[36] C. Ciminelli, F. Dell'Olio, V. M. N. Passaro, and M. N. Armenise, "Fully three-dimensional accurate modelling of scattering loss in optical waveguides," *Opt. Quant. Electron.*, vol. 41, pp. 285–298, 2009.
[37] R. Amatya, C. W. Holzwarth, H. I. Smith, and R. J. Ram, "Precision tunable silicon compatible microring filters," *IEEE Photon. Tech. Lett.*, vol. 20, no. 20, pp. 1739–1741, Oct. 2008.
[38] W. W. Lui, C. L. Xu, T. Hirono, K. Yokoyama, and W.-P. Huang, "Full-vectorial wave propagation in semiconductor optical bending waveguides and equivalent straight waveguide approximations," *J. Lightw. Technol.*, vol. 16, no. 5, pp. 910–914, May 1998.
[39] A. Yariv, "Universal relations for coupling of optical power between microresonators and dielectric waveguides," *Electron. Lett.*, vol. 36, pp. 321–322, 2000.
[40] F. Dell'Olio, D. Conteduca, C. Ciminelli, and M. N. Armenise, "New ultrasensitive resonant photonic platform for label-free biosensing," *Opt. Exp.*, vol. 23, pp. 28593–28604, 2015.
[41] R. C. Alferness and P. S. Cross, "Filter characteristics of codirectionally coupled waveguides with weighted coupling," *IEEE J. Quantum Electron.*, vol. QE-14, no. 11, pp. 843–847, Nov. 1978.
[42] R. Boeck, N. A. F. Jaeger, N. Rouger, and L. Chrostowski, "Series-coupled silicon racetrack resonators and the Vernier effect: Theory and measurement," *Opt. Exp.*, vol. 18, pp. 25151–25157, 2010.